Journal of Applied Remote Sensing

RemoteSensing.SPIEDigitalLibrary.org

Feasibility demonstration for calibrating Suomi-National Polar-Orbiting Partnership Visible Infrared Imaging Radiometer Suite day/night band using Dome C and Greenland under moon light

Shi Qiu
Xi Shao
Changyong Cao
Sirish Uprety

SPIE.

Shi Qiu, Xi Shao, Changyong Cao, Sirish Uprety, "Feasibility demonstration for calibrating Suomi-National Polar-Orbiting Partnership Visible Infrared Imaging Radiometer Suite day/night band using Dome C and Greenland under moon light," *J. Appl. Remote Sens.* **10**(1), 016024 (2016), doi: 10.1117/1.JRS.10.016024.

Feasibility demonstration for calibrating Suomi-National Polar-Orbiting Partnership Visible Infrared Imaging Radiometer Suite day/night band using Dome C and Greenland under moon light

Shi Qiu,[a,*] Xi Shao,[a] Changyong Cao,[b] and Sirish Uprety[c]

[a]University of Maryland, Department of Astronomy, College Park, Maryland 20742, United States

[b]National Oceanic and Atmospheric Administration/National Environmental Satellite, Data, and Information Service/The Center for Satellite Applications and Research, College Park, Maryland 20742, United States

[c]Colorado State University, Cooperative Institute for Research in the Atmosphere, Fort Collins, Colorado 80523, United States

Abstract. The day/night band (DNB) of the Visible Infrared Imaging Radiometer Suite (VIIRS) onboard Suomi National Polar-orbiting Partnership (Suomi-NPP) represents a major advancement in night time imaging capabilities. DNB covers almost seven orders of magnitude in its dynamic range from full sunlight to half-moon. To achieve this large dynamic range, it uses four charge-coupled device arrays in three gain stages. The low gain stage (LGS) gain is calibrated using the solar diffuser. In operations, the medium and high gain stage values are determined by multiplying the gain ratios between the medium gain stage, and LGS, and high gain stage (HGS) and LGS, respectively. This paper focuses on independently verifying the radiometric accuracy and stability of DNB HGS using DNB observations of ground vicarious calibration sites under lunar illumination at night. Dome C in Antarctica in the southern hemisphere and Greenland in the northern hemisphere are chosen as the vicarious calibration sites. Nadir observations of these high latitude regions by VIIRS are selected during perpetual night season, i.e., from April to August for Dome C and from November to January for Greenland over the years 2012 to 2013. Additional selection criteria, such as lunar phase being more than half-moon and no influence of straylight effects, are also applied in data selection. The lunar spectral irradiance model, as a function of Sun–Earth–Moon distances and lunar phase, is used to determine the top-of-atmosphere reflectance at the vicarious site. The vicariously derived long-term reflectance from DNB observations agrees with the reflectance derived from Hyperion observations. The vicarious trending of DNB radiometric performance using DOME-C and Greenland under moon light shows that the DNB HGS radiometric variability (relative accuracy to lunar irradiance model and Hyperion observation) is within 8%. Residual variability is also discussed. © *2016 Society of Photo-Optical Instrumentation Engineers (SPIE)* [DOI: 10.1117/1.JRS.10.016024]

Keywords: Suomi-National Polar-Orbiting Partnership/Visible Infrared Imaging Radiometer Suite day/night band; day/night band calibration; night time vicarious calibration; lunar calibration; lunar irradiance; Dome C; Greenland.

Paper 15219 received Mar. 19, 2015; accepted for publication Jan. 5, 2016; published online Mar. 11, 2016.

1 Introduction

The Visible Infrared Imaging Radiometer Suite (VIIRS) is one of the key instruments onboard the Suomi National Polar-Orbiting Partnership (Suomi-NPP) spacecraft, which was successfully launched on October 28, 2011. The VIIRS nadir door was opened on November 21, 2011, which enables a new generation of operational moderate resolution-imaging capabilities following

*Address all correspondence to: Shi Qiu, E-mail: sqiu1@umd.edu

the legacy of the advanced very high resolution radiometer on the National Oceanic and Atmospheric Administration and the moderate-resolution imaging spectroradiometer (MODIS) on Terra and Aqua satellites. The VIIRS empowers operational environmental monitoring and numerical weather forecasting, with 22 imaging and radiometric bands including 14 reflective solar bands (RSB), seven thermal emissive bands, and one day-night band (DNB) covering wavelengths from 0.41 to 12.5 microns, providing the sensor data records (SDR) for more than 20 environmental data points including clouds, sea surface temperature, ocean color, polar wind, vegetation fraction, aerosol, fire, snow and ice, vegetation, and other applications with its calibrated and geolocated SDR.[1–3]

The DNB sensor of the VIIRS detects radiance in a panchromatic visible/near-infrared (Vis/NIR) band (0.5 to 0.9 μm). It shares the same optical path with the Vis/NIR focal plane array (FPA), but uses a unique detector technology. The DNB represents a major advancement in night time imaging capabilities, it surpasses its predecessor the operational linescan system on the Defense Meteorological Satellite Program in radiometric accuracy, spatial resolution, and geometric quality.[4–6] The primary mission of the DNB is to provide imagery of clouds and other Earth features over illumination levels ranging from full sunlight to half-moon. Other applications of using DNB such as light outage detections during major storms[1] have also been recently demonstrated.

Additionally, the DNB sensor of the VIIRS utilizes a backside-illuminated charge coupled device FPA for sensing radiances spanning seven orders of magnitude in one panchromatic (0.5 to 0.9 μm) RSB. In order to cover this extremely broad measurement range, the DNB employs four imaging arrays that comprise three gain stages: the low gain stage (LGS), the medium gain stage (MGS), and the high gain stage (HGS) with two arrays. A gain-selection algorithm is implemented onboard that determines which stage's output should be used for each pixel. The HGS produces imagery of night scenes, and it is actually made of two separate arrays of identical design: high gain stage A and high gain stage B. The LGS produces imagery of the brightest Earth scenes such as sunlit clouds. The MGS produces imagery of scenes near the terminator or at twilight. Two arrays are used for HGS to minimize the probability that a radiation event may corrupt the measurement of a night scene.[7] The basic parameters and key DNB characteristics that define its performance are listed in Table 1 (also see Ref. 8).

The DNB raw data record is calibrated into SDR. Generation of the SDR requires accurate knowledge of the dark offsets and gain coefficients for each DNB stage. The typical frequencies for onboard offsets are updated about monthly.[7] These are measured on-orbit and stored in lookup tables that are used during ground processing. The format of the values in the ground tables differ for the offset and gain tables. The offsets are organized into a matrix that has four dimensions. The first dimension is the number of samples and has 4064 elements, and the second

Table 1 DNB design specifications.

DNB Characteristics	Specification	Prelaunch performance	On-orbit performance
Spectral passband center[8]	700 ± 14 nm	707 nm	Model estimate: 694 nm
Spectral passband bandwidth[8]	400 ± 20 nm	379 nm	Model estimate: 375 nm
Dynamic range ($Wcm^{-2}\,sr^{-1}$)[8]	3×10^{-9} to 0.02	3×10^{-9} to 0.021	3×10^{-9} to 0.0186
Calibration uncertainty (HGS)	30%	11%	15%
SNR@ < 53 deg SNR@ ≥ 53 deg[8]	≥6 at L_{min} ≥5 at L_{min}	>10 across scan	>9 across scan
Number of bits in A/D	14 bits (16,384 levels) for HGS; 13 bits (8192 levels) for MGS and LGS		
Relative radiometric gains	119,000: 477: 1 (HGS: MGS: LGS)		
Aggregation	32 aggregation zones		
Time delay integration	1, 3, and 250 pixels for LGS, MGS, and HGS, respectively		
Number of samples per scan	4064		

dimension is the number of detectors and has 16 elements. The third dimension is the number of gain stages and has three elements, one for each of the LGS, MGS, and HGS stage. The fourth dimension is the half angle mirror (HAM) side and has two elements, one for HAM side A and one for HAM side B. The gains are organized into a matrix that has five dimensions. The first dimension is the number of electronic sides and has two elements; the second is the number of aggregation zones and has 32 elements, the third is the number of detectors and has 16 elements, the fourth is the number of gain stages and has three elements, and the fifth is the coefficient type and has three elements.[7] The LGS gain values are determined by solar diffuser data (also known as the onboard calibration). While the reflective solar bands of VIIRS have been calibrated regularly during daytime using solar light reflected from the onboard solar diffuser, the vicarious calibration of HGS of DNB requires the usage of light sources at night. Since the three gain stages together cover the entire required radiance range of DNB with sufficient overlap, the LGS values are determined by using data collected from the solar diffuser, the MGS and HGS values are determined by multiplying the LGS gains by the MGS/LGS and HGS/MGS gain ratios, respectively.[8–10]

The MGS and HGS cannot be calibrated directly using solar diffuser data because these gain stages saturate at solar diffuser illumination levels. The Moon is a natural light source at night and is also predictable. It can be used to perform vicarious calibration of DNB when it illuminates the ground calibration site.[9] While the radiometric property of solar light is quite stable and can be well characterized by solar irradiance model such as in Ref. 10, the lunar light is a strong function of Sun–Earth geometry, lunar phase, and liberation.[11] Models to characterize the radiometric property of lunar light are still being developed.[11,12]

To evaluate the radiometric accuracy of DNB, Liao et al.[8] performed vicarious calibrations under lunar illumination using Railroad Valley Playa as the calibration targets from March to October of year 2012. The results show that the radiometric calibration uncertainty in HGS is about 15%. However, the relatively low reflectance of the targets, atmospheric effects such as variable moisture content, large uncertainty associated with straylight, and interference from the full moon all may contribute to the uncertainties.

In this paper, feasibility of using lunar illumination to perform vicarious radiometric validation of DNB at night over Dome C in Antarctic and Greenland in northern hemisphere is proposed. We selected events from years 2012 to 2014 that were recorded at nights with more than half-moon illumination and Suomi-NPP passing over the vicarious sites, to verify the radiometric accuracy of HGS of DNB. In contrast to Liao's paper[8] which only included events of nearby full moon, our analysis includes events with various lunar phases.

The calibration of DNB is performed using a lunar spectral irradiance model[12] as a function of Sun–Earth–Moon distances and lunar phase to determine the top-of-atmosphere (TOA) reflectance at the vicarious sites. The time series of vicariously-derived reflectance is analyzed and compared with reflectance derived from Hyperion observations. Limitations and challenges in our analysis are also discussed. This work helps to independently verify the radiometric accuracy of HGS of DNB.

2 Calibration Sites

The Antarctic Dome C site (75.1° S, 123.35° E) and Greenland site (74° N, 41° W) in the southern and northern hemisphere, respectively, are selected as region of interests (ROIs), shown in Fig. 1, and used to characterize the DNB radiance measurement. The size of the ROIs radius is about 50 km.

In searching for vicarious calibration sites for satellite observations, many factors need to be considered, including the atmospheric turbulence, cloud cover, precipitable water vapor, thermal emission from the atmosphere, auroral activity, aerosol/dust pollution, average and maximum wind speed, seismic activity, rates of snow/rain fall, light pollution, accessibility, infrastructure, and cost of operation. The Dome C site is a large snow flat located in Antarctica at a high altitude of 3.25 km. The site is very cold and dry with temperatures ranging from −23°C to −83°C. It has very low atmospheric absorption with unique characteristics such as: being spatially highly uniform, high altitude; high reflectance; low water vapor content, and low aerosol and dust content.[15,16] It is one of the Committee on Earth Observation Satellites endorsed vicarious

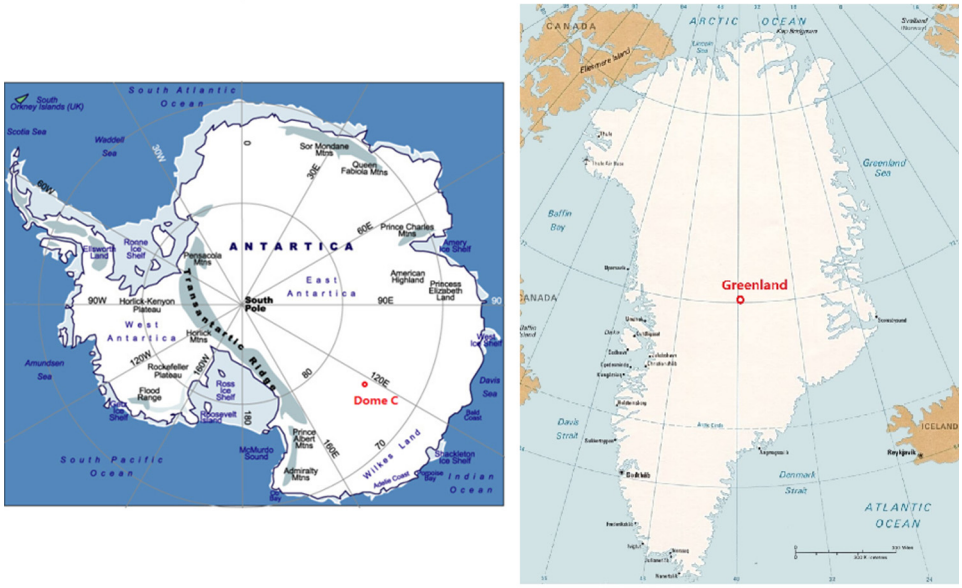

(a) Dome C (b) Greenland

Fig. 1 Locations of vicarious sites [(a) Dome C and (b) Greenland] in the southern and northern hemisphere, respectively.[13,14]

calibration sites. On the other hand, Dome C site shows significant bidirectional reflectance distribution function (BRDF) effect at high lunar zenith angles.[15–20] Additionally, due to the limitation that only a few DNB observations of Dome C with sufficient lunar illumination and nadir-pass by Suomi-NPP exist, modeling of BRDF and seasonal effect may not be accurate, and hence this paper referenced previous articles[18] to suggest the effects.

Vicarious calibrating HGS of DNB requires lunar illumination over the calibration site, which occurs at night. The two ROIs from which we selected cases are located at high latitude, and consequently experience perpetual nights during half of the year. For Antarctic Dome C, this occurs during May to August each year.[15,16] For Greenland, as another site in the northern hemisphere having similar characteristics as Dome C site, this occurs during the winter season from November to January. The DNB observation of Greenland can be used to complement the data gap. Both sites have thin and relatively constant atmospheres; the sky in these sites are clear most of the time. These two sites have also been used in numerous studies in the past for sensor calibration and validation.

3 Methodology

Two vicarious calibration sites, i.e., Dome C and Greenland, have been investigated in this study using DNB observations. Figure 2 shows examples of the DNB observations when Suomi-NPP flew over the ROIs. The overall procedures of analysis are: selection of observations, deriving characteristic radiance from DNB observations, deriving TOA reflectance for ROIs using lunar irradiance model, and comparison with TOA reflectance for ROIs derived from Hyperion observations. Details of the analysis method are illustrated as follows.

3.1 *Selection of Typical Observations*

The guideline for event selection is to identify events with overpass of Suomi-NPP, with sufficient lunar illumination and no solar light contamination. In selecting observations, attention needs to be paid to terminator straylight effect on the instrument due to solar illumination after the satellite passes through the day-night terminator projected on Earth's surface. This effect is more significant during a solstice. Figure 2 shows DNB observation of Dome C and Greenland with lunar illumination, respectively. The selection criteria are summarized as follows.

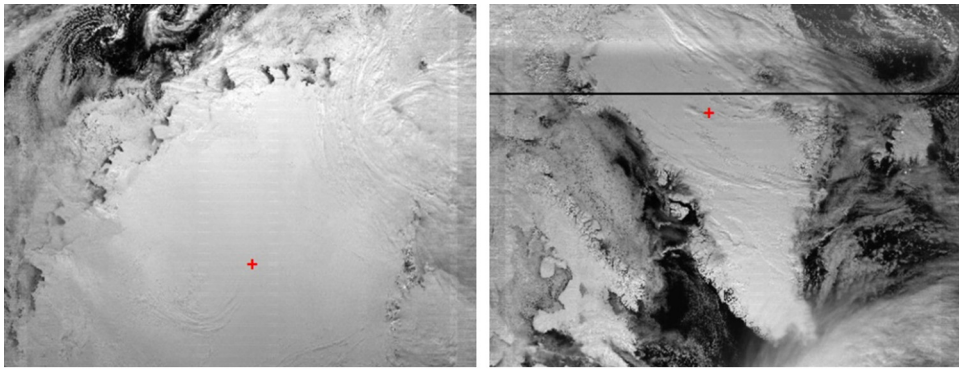

(a) 7/4/2012 15:05 (Dome C) (b) 11/30/2012 6:01 (Greenland)

Fig. 2 (a) DNB observation of Dome C and (b) DNB observation of Greenland Red '+' mark the centers of the vicarious sites used in this study. The solar zenith angles at the ROIs are 127.37 deg and 120.86 deg for panels a and b, respectively.

a. Suomi-NPP overpasses the ROIs, i.e., the nadir distance to the center of ROIs is <10 km. For the observations we have identified, the angle between the nadir and the normal of the surface of ROIs is less than about 4 to 5 deg given the size of ROI radius of about 50 km. This reduces the uncertainty due to the variations in the satellite-view angle toward the ROIs.
b. The absolute value of lunar phase angle is less than 90 deg (half-moon), i.e., lunar phase is larger than the half-moon. This condition ensures that adequate lunar light illuminates over the vicarious sites. In this study, the illumination by the Moon is assumed to be dependent on the absolute value of the lunar phase angle, regardless of whether the Moon is waxing or waning. In this way, the lunar irradiance model MT2009 can be applied directly.
c. Lunar zenith angle is less than 80 deg.
d. Solar zenith angle is larger than 118 deg. This assures that the overpass of Suomi-NPP occurs at night and there are no influences of stray light effects present at the selected ROIs during the observations.

For Dome C, an ROI is a section of radius equal to 50 km centered area located around 74.50° S latitude and 123.35° E longitude. For Greenland, a ROI with a size of nearly 50 km in radius is located around 74° N latitude and 41° W longitude.

Figure 3 shows time series of lunar zenith angle, solar zenith angle, and lunar phase angle for the cases we identified over Dome C and Greenland, which satisfy the selection criteria. In total, there are 27 cases identified for Dome C over the periods April to August, 2012 and April to August, 2013. Sixteen cases are identified for Greenland over the period from November, 2012 to January, 2013 and from November, 2013 to January, 2014 when Suomi-NPP passes Greenland. We selected the solar zenith angle larger than 118 deg, to avoid influences of stray light effects. The threshold value (the black line) for solar zenith angle is 118 deg, the threshold value for lunar zenith angle (the blue line) is 80 deg, and the threshold value (the red line) for the absolute value of lunar phase angle is 90 deg.

Figure 4 shows the radiance values at Dome C site from DNB observations under different lunar phases; it can be clearly seen that the Dome C region varies from bright to dark as the lunar phase changes from nearly full moon to close to half-moon.

3.2 *Day-Night Band Data Analysis*

Each TOA radiance data from DNB observations is extracted using the following steps:

a. Radiance data from DNB observations are collected for all selected cases as in Sec. 3.1.
b. Once all the radiance data within an ROI is extracted, radiance data within the ROI is processed to derive mean TOA radiance L_{DNB} and its standard deviation σ_{DNB}. L_{DNB} is regarded as the characteristic radiance for the ROI.

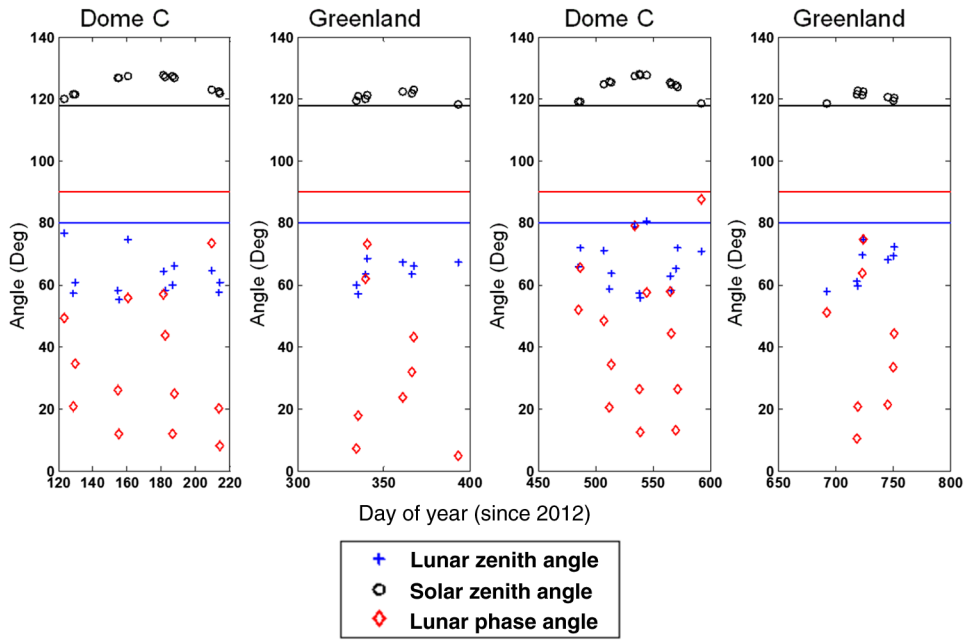

Fig. 3 Time series of lunar zenith angle, solar zenith angle, and lunar phase angle for the observations satisfying the selection criteria over Dome C (the first and third panels from left) and Greenland (the second and fourth panels from left). The horizontal lines mark the thresholds for the corresponding selection criteria.

3.3 *Lunar Irradiance Model*

The amount of moonlight available to illuminate the surface of the Earth depends on Sun–Moon–Earth geometry, lunar phase (ranging from a new to full moon) and lunar elevation in the sky, and it is not a linear function of the lunar phase.[11] In this paper, we use a TOA spectral lunar irradiance model Miller and Turner[12] to quantify the effects of lunar radiation on DNB observation. Miller and Turner 2009 (MT2009) is developed in preparation of calibrating night time low-light measurements from DNB to enable quantitative nighttime multispectral applications. The model uses solar source observations, lunar spectral albedo data, and accounts for the time-varying Sun/Earth/Moon geometry and lunar phase. It produces 1-nm resolution irradiance spectra over the spectral interval of 0.3 to 1.2 μm for any given lunar phase. In

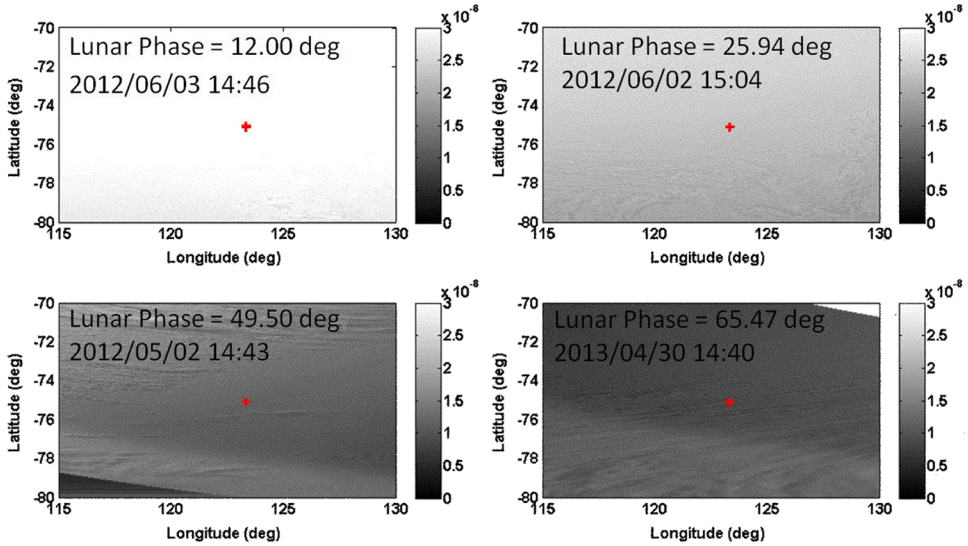

Fig. 4 Dome C from DNB observations under different lunar phases (unit: W/cm^2/sr).

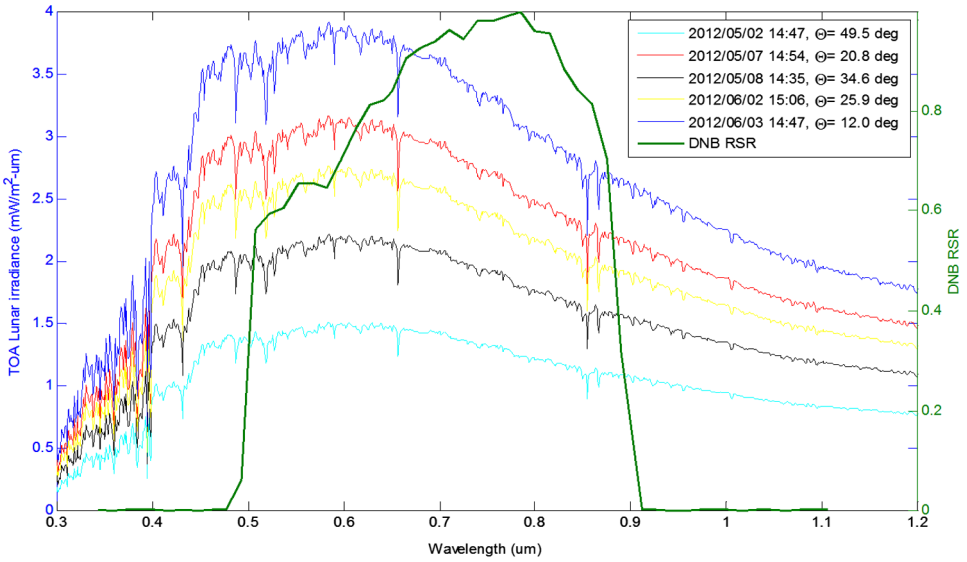

Fig. 5 TOA lunar spectral irradiance modeled from MT2009 for five cases satisfying the event-selection criteria with different lunar phase angles together with RSR of DNB.

this model, the scattering property of the lunar surface is assumed to be Lambertian. The uncertainties attached to the model, including the geocentric assumption of the standard geometry model, range from 7% to 12% for typical observing conditions.[12] The model has been benchmarked against lunar observations such as the Sea-viewing Wide Field-of-view Sensor, MODIS-Aqua satellites, and the robotic lunar observatory lunar irradiance model.[11]

Figure 5 shows the TOA lunar spectral irradiance modeled from MT2009 for five cases satisfying the event selection criteria with different lunar phase angles together with the spectral response function (SRF) of DNB. It can be seen that lunar irradiance depends strongly on the lunar phase.

To compute the TOA lunar radiance L_{MT2009} above the ROI sites, we use the formula

$$L_{\mathrm{MT2009}} = \frac{E_m}{\pi} \cos(\theta_m), \tag{1}$$

where θ_m is the lunar zenith angle. E_m is the downwelling TOA lunar irradiance derived from the MT2009 model and weighted by the sensor spectral response function, i.e.,

$$E_m = \frac{\int_{\lambda_1}^{\lambda_2} I_{\mathrm{MT}}(\lambda)\mathrm{SRF}(\lambda)\mathrm{d}\lambda}{\int_{\lambda_1}^{\lambda_2} \mathrm{SRF}(\lambda)\mathrm{d}\lambda}, \tag{2}$$

where $I_{\mathrm{MT}}(\lambda)$ is the lunar irradiance spectra calculated from MT2009 model for a specific date and accounts for the Sun–Moon and Moon–Earth distance such as those shown in Fig. 5. $\mathrm{SRF}(\lambda)$ is the spectral response function of the DNB sensor. It is noted that when the Moon is below the horizon, i.e., lunar zenith angle $\theta_m > 90$ deg, the contribution of lunar radiance is zero. The DNB-band-averaged TOA reflectance ρ for the ROI is calculated using

$$\rho_{\mathrm{DNB}} = L_{\mathrm{DNB}}/L_{\mathrm{MT2009}}. \tag{3}$$

Figure 6 shows RSR of DNB and an example of total lunar irradiance as derived from MT2009 lunar irradiance model for the data we collected; there is a change of DNB RSR in April 2, 2013 to account for the mirror degradation of VIIRS.[2] This change in DNB RSR causes an increase of 3% to 4% in lunar radiance.

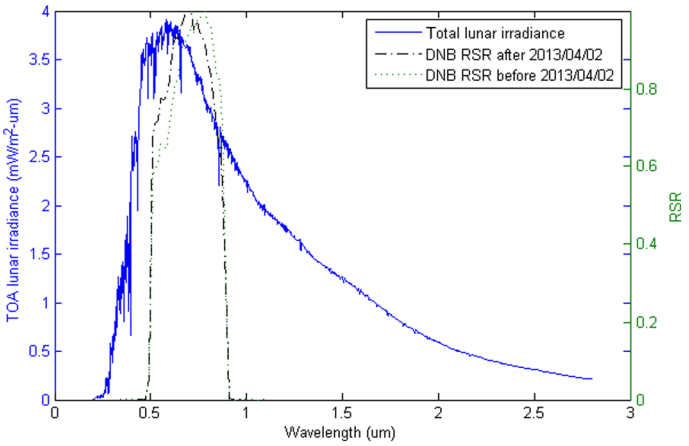

Fig. 6 DNB RSRs and total lunar irradiance for ROIs as derived from MT2009 lunar irradiance model.

3.4 *Characteristics of Vicarious Sites Reflectance*

In this paper, the DNB-wavelength range-averaged reflectance from Hyperion observations of the vicarious calibration sites of interest is derived to serve as a reference for comparison with the TOA reflectance derived from DNB observations. The EO-1 Hyperion is a hyperspectral sensor launched by NASA on November 21, 2000, which images the Earth in 242 spectral bands with wavelengths ranging from 0.35 to 2.57 μm. Hyperion is a push broom sensor and has a footprint size of 30 m and the swath width of 7.5 km.[21] The radiometric stability of the instrument is maintained using solar, lunar, and in-flight calibration sources. The Hyperion data in counts are converted to reflectance by first converting the DN values to the spectral radiance (using a scaling coefficient 40 for Vis/NIR and 80 for short-wave infrared band) and converting the spectral radiance to reflectance using the solar exoatmospheric irradiance at 1 AU.[18] The Hyperion spectral response over the given sites can be convolved with the instrument SRFs, i.e., SRFs of DNB in this study, to derive the DNB-band-averaged TOA reflectance ρ_{Hyp} over the vicarious sites.

For this study, nine Hyperion data sets over Dome C and five data sets over Greenland were collected and analyzed. The data used in the analysis have solar zenith angles ranging from nearly 50 deg to 65 deg. All of these data are at nadir viewing. However the solar zenith angle varies. It is demonstrated in previous studies, such as Uprety and Cao,[18] that the bidirectional effects over Dome C snow for near-nadir measurements are dominated by solar zenith angle variation. The solar zenith angles of Hyperion observations analyzed are in similar range when compared to lunar zenith angles during DNB observations. From Fig. 7, we can derive the value of reflectance from Hyperion observations ρ_{Hyp} for Dome C and Greenland before and after April 2, 2013, respectively, as shown below:

$$\rho_{\mathrm{Dome\,C,Hyp}} = 0.867 \pm 0.0081, \rho_{\mathrm{Greenland,Hyp}} = 0.884 \pm 0.0253 \text{ before April 2, 2013;}$$
$$\rho_{\mathrm{Dome\,C,Hyp}} = 0.868 \pm 0.0083, \rho_{\mathrm{Greenland,Hyp}} = 0.886 \pm 0.0251 \text{ after April 2, 2013.}$$

Nine Hyperion data sets over Dome C and five data sets over Greenland are analyzed in this paper. Illumination geometries for Dome C range from 50 deg to 65 deg whereas that for Greenland three out of five datasets have solar zenith nearly 50 deg. The other two data have solar zenith at nearly 54 deg and 60 deg. Thus, the illumination geometry differences are one of the major reasons for differences observed between Dome C and Greenland spectrum. In addition, the differences in spectrum are also caused by the seasonal effects of snow surface between Dome C and Greenland.

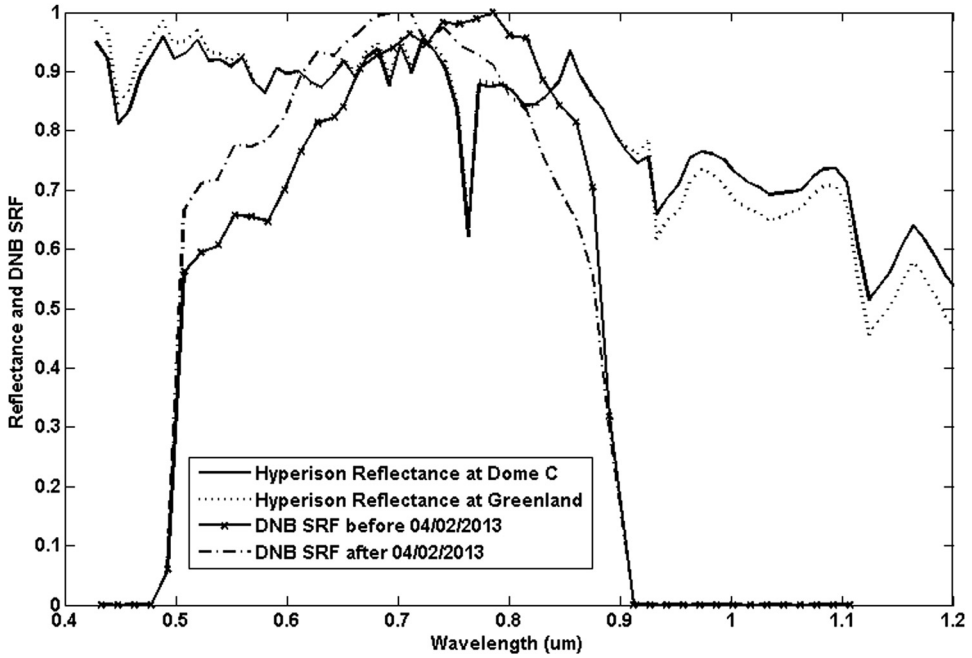

Fig. 7 Spectral reflectance for Dome-C and Greenland as derived from Hyperion observations along with spectral response functions for VIIRS DNB.

4 Results and Discussion

4.1 *Analysis of Day Night Band Observation over Dome C and Greenland*

The radiance data from DNB observations for the selected events over the year 2012 and 2014 were collected and analyzed following procedures outlined in Sec. 3 to derive the characteristic radiance L_{DNB} and reflectance ρ_{DNB} for the ROIs. Figure 8 shows the scatter plot of measurement TOA radiance of Dome C and Greenland observed by DNB versus the predicted TOA radiance from the MT2009 model. In predicting the TOA radiance for the ROIs, the modeled radiance L_{MT2009} has been multiplied with the reflectance derived from the Hyperion observations, i.e., $\rho_{\mathrm{Dome\,C,Hyp}}$ and $\rho_{\mathrm{Greenland,Hyp}}$, respectively. The coefficient of determination R^2 for modeled radiance versus observed radiance is 0.989 and root-mean-square-error = 0.529. This confirms that lunar illumination on the Earth can be used as a light source for effective vicarious calibration of DNB.

We further investigated the evolution of reflectance ρ_{DNB} so that we can assess radiometric stability of DNB. Figure 9 shows the time series of reflectance for Dome C during year 2012 to 2013 and Greenland during year 2012 to 2014. It can be seen that the reflectance fluctuates over time. We calculated the mean reflectance over the four time periods and obtain $\bar{\rho}_{\mathrm{Dome\,C,DNB}} = 0.891 \pm 0.033$ for May to August, 2012; $\bar{\rho}_{\mathrm{Greenland,DNB}} = 0.892 \pm 0.023$ for November, 2012 to January, 2013; $\bar{\rho}_{\mathrm{Dome\,C,DNB}} = 0.919 \pm 0.023$ for the period from March to August, 2013; $\bar{\rho}_{\mathrm{Greenland,DNB}} = 0.875 \pm 0.043$ for November, 2013 to January, 2014. The potential difference between the reflectance determined by Hyperion and VIIRS as observed in Table 2 are mainly caused by a number of factors such as viewing geometry differences, uncertainty in lunar irradiance, very limited number of DNB datasets, calibration uncertainties in both Hyperion and DNB, registration errors (since the Hyperion region of interest used in this paper is 1.5 km × 1.5 km compared to 50 km × 50 km of DNB), and atmospheric variability, since the Hyperion and DNB observations are not in-situ measurements. Although there is 2% to 3% increase in radiance for DNB band after the implementation of SRF change for DNB in April, 2013 to correct for VIIRS mirror degradation, the variation of reflectance due to this SRF change is small.

As seen in Fig. 9, there are still significant variations in the time series of reflectance ρ_{DNB} derived from DNB observation. The large deviations are mainly due to the limited number of

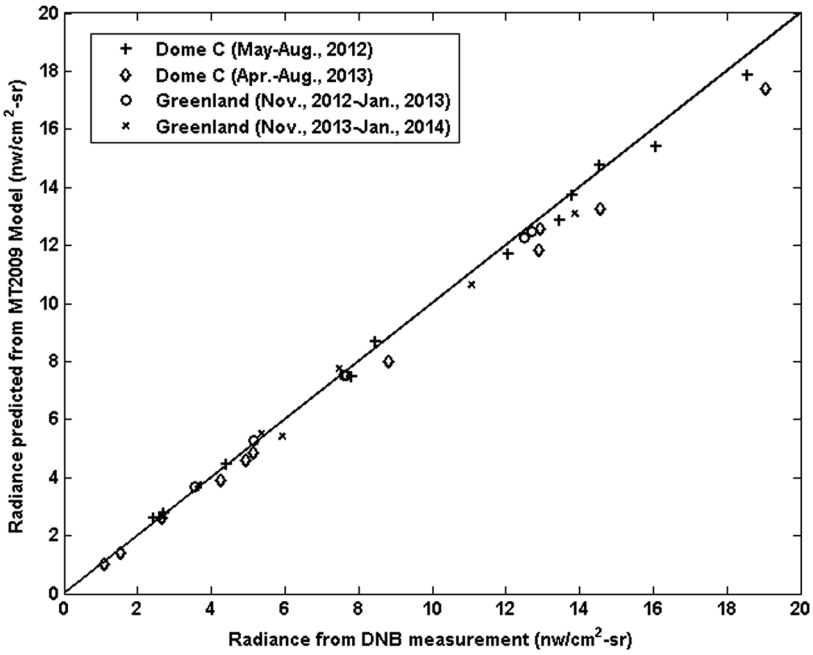

Fig. 8 Scatter plot of radiances observed by DNB versus radiance predicted from MT2009 model.

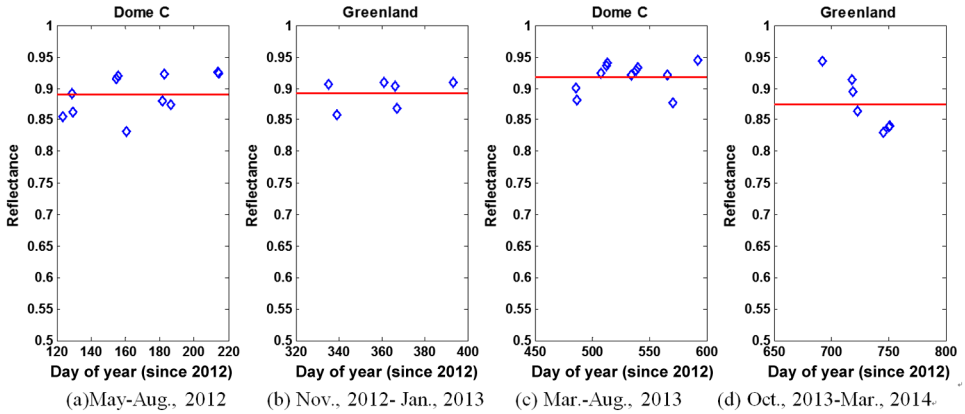

Fig. 9 Time series of reflectance for Dome C and Greenland as derived from DNB observations.

Table 2 TOA reflectance derived from DNB observations over four periods.

	Dome C (May to August, 2012)	Greenland (November, 2012 to January, 2013)	Dome C (May to August, 2013)	Greenland (October, 2013 to March, 2014)
ρ_{Hyperion}	0.867 ± 0.008	0.884 ± 0.025	0.868 ± 0.008	0.886 ± 0.025
Mean ρ_{DNB}	0.891 ± 0.033	0.892 ± 0.023	0.919 ± 0.023	0.875 ± 0.043
Mean $\rho_{\text{DNB}}/\rho_{\text{Hyperion}}$	$1.027 \pm 3.92\%$	$1.009 \pm 3.86\%$	$1.058 \pm 2.82\%$	$0.987 \pm 5.6\%$
Range of $\rho_{\text{DNB}}/\rho_{\text{Hyperion}} - 1$	(−6.1%, 4.5%)	(−3.8%, 2.0%)	(−1.3%, 6.3%)	(−7.6%, 5.0%)

data samples over ROIs. Due to the limitation that only few DNB observations exist, modeling of BRDF and seasonal effect may not be accurate, and hence the authors have referenced previous articles to suggest the effects. In addition, there is uncertainty in DNB SRF, lunar model used, variations in nighttime atmospheric conditions, atmospheric absorption to lunar lights, and uncertainty embedded in lunar radiance estimation. One of the major attributing factors can be that the TOA reflectance is a function of the lunar and sensor view geometry, which is generally referred to as BRDF. BRDF depends on lunar zenith angle, sensor zenith angle, and lunar and sensor relative azimuth angle. However, for nadir viewing, BRDF is dominated by lunar zenith angle. For example, Uprety and Cao[18] has shown the BRDF uncertainty of 5% with nadir viewing and solar zenith limited to less than 70 deg from MODIS observation. Figure 10 shows the dependence of reflectance ρ_{DNB} as derived from DNB observations for Dome C and Greenland versus lunar zenith angle. There is an overall trend of decrease in reflectance as the lunar zenith angle increases. This relationship is consistent with the relation for reflectance versus illumination zenith angle as presented in the analysis of MODIS observation for Dome C.[18] However DNB observations over Dome C have lunar zenith angles with upper limit close to 80 deg, which is larger than that in Uprety and Cao[18] with MODIS data. Thus the min–max variation in reflectance time series can be observed on the order of 10%.

In the left panel of Fig. 10, the variation of reflectance for 2012 and 2013 is more than 10% and depends strongly on lunar zenith angle, which is likely due to model uncertainties, BRDF of snow, SRF changes, and atmospheric conditions. Therefore, the dependence of BRDF for the vicarious site on lunar zenith angle can help reduce the variability in the reflectance ρ_{DNB}. The left panel in Fig. 10 also reconfirms that the derived reflectance ρ_{DNB} of Dome C over May to June, 2013 is larger than that over May to August, 2012 even after the dependence on the lunar zenith angle has been taken into account. Additional factors such as uncertainty in the lunar irradiance model and variations in the atmospheric absorption to lunar lights transmitted through the atmosphere can also contribute to uncertainties in the derived reflectance ρ_{DNB}. For example, the lunar irradiance model used in this study does not differentiate the waxing and waning phase of the Moon, which can have significantly different lunar irradiances for certain Sun–Moon–Earth geometries. In the right panel of Fig. 10, the trend is not consistent over Greenland. There could be a number of factors as BRDF, seasonal effect, calibration uncertainties and more.

As indicated from results, the DNB HGS radiometric variability relative accuracy to lunar irradiance model and Hyperion observation is within 8%. The difference between the residual

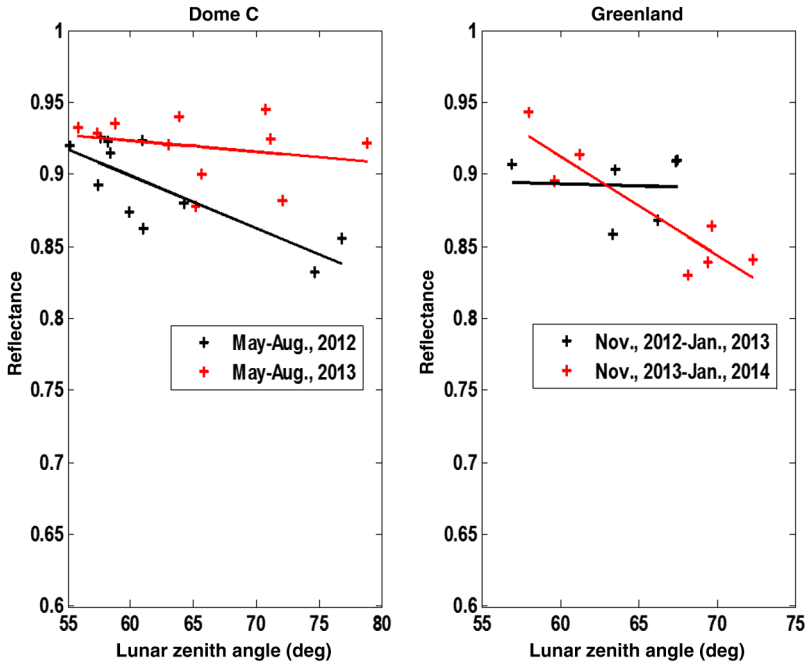

Fig. 10 Reflectance versus lunar zenith angle as derived from DNB observations for Dome C and Greenland.

variability of our analysis and that of the Liao et al.'s[8] analysis can be attributed to a number of differences between the two studies. First, the duration of the two studies is different; our analysis took places between the years 2012 to 2014 (the year 2014 is only for Greenland), while the Liao et al.'s[8] analysis took data in a much shorter duration of March to October, 2012. Second, the vicarious site selection also varied, with our vicarious site located at Dome C/Greenland, while the vicarious site in the Liao et al.'s[8] analysis was located at Railroad Valley our study excluded events of straylight effect but the Liao et al.'s[8] analysis accounts for these events and performed straylight corrections. Our analysis was conducted in various lunar stages, and theirs were conducted at near full moon. Our analysis also utilized a different lunar irradiance model from the Liao et al.'s[8] analysis. All these aspects combined can produce a discrepancy in the two residual variability values of the respective studies.

4.2 *Limitations of this Study*

There exist a number of limitations in this study. Number of DNB observations available for applying the model is very limited. The effect can be seen especially for Greenland during November 2012 to January 2013. The trend for this time series over Greenland is not consistent with that over Dome C. The major reason as explained earlier is the limited number of data points. Even one data point out of five can change the trend significantly. Similarly, large uncertainty exists in lunar model used to compute lunar irradiance. DNB RSR degradation is a continuous function of time. However, this study uses only two versions of DNB RSRs. One is prelaunch that is used for data before April 2013 and the other is modulated RSR generated on April 04, 2013. This adds uncertainty in Hyperion reflectance, since only two RSRs are used rather than time-dependent continuous function of RSR. Other factors such as uncertainty due to BRDF effects, atmospheric absorption variability between Hyperion and DNB observations due to lack of in-situ measurements have not been accounted. In addition, the absolute calibration uncertainties of reference sensor, i.e., Hyperion in this study, have not been accounted. These uncertainties are valid for both sites. Nevertheless, the radiometric uncertainty in the DNB HGS determined from observation with moon light is ~8% and is much less when compared to the requirement accuracy of 30%.

5 Conclusions

The feasibility of using lunar illumination to perform vicarious radiometric calibration of DNB at night is proposed in this paper. We developed systematic procedures of selecting observations, deriving characteristic radiance from DNB observations for ROIs such as Dome C and Greenland, and deriving TOA reflectance for ROIs using the lunar irradiance model. The vicariously derived mean reflectance from DNB observations over the four time periods are $\bar{\rho}_{\text{Dome C,DNB}} = 0.891 \pm 0.033$ for May to August, 2012; $\bar{\rho}_{\text{Greenland,DNB}} = 0.892 \pm 0.023$ for November, 2012 to January, 2013; $\bar{\rho}_{\text{Dome C,DNB}} = 0.919 \pm 0.023$ for the period from March to August, 2013; $\bar{\rho}_{\text{Greenland,DNB}} = 0.875 \pm 0.043$ for November, 2013 to January, 2014 based on the R^2 argument. It agrees with the reflectance derived from Hyperion observations. There are remaining uncertainties in the estimated reflectance from DNB observations and these uncertainties can be due to BRDF effects, seasonal effects, uncertainty on SRF, lunar model uncertainty, variations in nighttime atmospheric conditions, atmospheric absorption to lunar lights, and uncertainty embedded in lunar radiance estimation. A more accurate lunar irradiance model as well as a more accurate method of accounting for atmospheric absorption can help improve the accuracy of the vicarious calibration of HGS of DNB. There are still other properties have to be characterized and evaluated in future studies.

Acknowledgments

The authors would like to thank Ms. Yan Bai for the assistance with data acquisition. We also thank Dr. S. Miller for making his lunar irradiance model publicly available. This study was partially funded by the Joint Polar Satellite System program. The manuscript contents are solely

the opinions of the authors and do not constitute a statement of policy, decision, or position on behalf of NOAA or the U.S. government.

References

1. C. Cao, X. Shao, and S. Uprety, "Detecting light outages after severe storms using the S-NPP/VIIRS day/night band radiances," *IEEE Geosci. Remote Sens. Lett.* **10**(6), 1582–1586 (2013).
2. C. Cao et al., "Early On-orbit performance of the visible infrared imaging radiometer suite onboard the Suomi National Polar-Orbiting Partnership (S-NPP) satellite," *IEEE Trans. Geosci. Remote Sens.* **52**(2), 1142–1156 (2014).
3. H. Letu et al., "Estimating energy consumption from night-time DMPS/OLS imagery after correcting for saturation effects," *Int. J. Remote Sens.* **31**(16), 4443–4458 (2010).
4. T. E. Lee et al., "The NPOESS VIIRS day/night visible sensor," *Bull. Am. Meteorol. Soc.* **87**(2), 191–199 (2006).
5. S. D. Miller et al., "Suomi satellite brings to light a unique frontier of nighttime environmental sensing capabilities," *Proc. Natl. Acad. Sci. U. S. A.* **109**(39), 15706–15711 (2012).
6. S. Lee et al., "A new method for Suomi-NPP VIIRS Day #x2013;night band on-orbit radiometric calibration," *IEEE Trans. Geosci. Remote Sens.* **53**(1), 324–334 (2015).
7. J. Geis et al., "VIIRS day-night band gain and offset determination and performance," *Proc. SPIE* **8510**, 851012 (2012).
8. L. B. Liao et al., "Suomi NPP VIIRS day-night band on-orbit performance," *J. Geophys. Res. Atmos.* **118**(22), 12705–12718 (2013).
9. S. Mills, S. Weiss, and C. Liang, "VIIRS day/night band (DNB) stray light characterization and correction," *Proc. SPIE* **8866**, 88661P (2013).
10. G. Thuillier et al., "The solar spectral irradiance from 200 to 2400 nm as measured by the SOLSPEC spectrometer from the ATLAS and EURECA Missions," *Sol. Phys.* **214**, 1–22 (2003).
11. H. H. Kieffer and T. C. Stone, "The spectral irradiance of the moon," *Astron. J.* **129**(6), 2887–2901 (2005).
12. S. D. Miller and R. E. Turner, "A dynamic lunar spectral irradiance data set for NPOESS/VIIRS day/night band nighttime environmental applications," *IEEE Trans. Geosci. Remote Sens.* **47**(7), 2316–2329 (2009).
13. "Map of Antarctica Messner Route to South Pole," 3 Below Zero, http://3belowzero.com/3belowzero-expedition-details/attachment/antar1/ (1 October 2014).
14. "Maps of Scandinavia," About, http://goscandinavia.about.com/od/scandinaviatripplanning/ig/Scandinavia-Maps/Relief-Map-of-Greenland.htm (1 October 2014).
15. C. Cao et al., "Establishing the Antarctic Dome C community reference standard site towards consistent measurements from Earth observation satellites," *Can. J. Remote Sens.* **36**(5), 498–513 (2010).
16. S. Uprety and C. Cao, "Radiometric and spectral characterization and comparison of the Antarctic Dome C and Sonoran Desert sites for the calibration and validation of visible and near-infrared radiometers," *J. Appl. Remote Sens.* **6**(1), 063541 (2012).
17. J. S. Lawrence et al., "Exceptional astronomical seeing conditions above Dome C in Antarctica," *Nature* **431**(7006), 278–281 (2004).
18. S. Uprety and C. Cao, "A comparison of the Antarctic Dome C and Sonoran Desert sites for the cal/val of visible and near infrared radiometers," *Proc. SPIE* **7811**, 781106 (2010).
19. S. Uprety and C. Cao, "Using the Dome C site to characterize AVHRR near-infrared channel for consistent radiometric calibration," *Proc. SPIE* **8153**, 81531Y (2011).
20. S. Qiu et al., "Vicarious validation of straylight correction for VIIRS day/night band using Dome-C," *Proc. SPIE* **9607**, 96072H (2015).
21. D. E. Lencioni et al., "The EO-1 advanced land imager: an overview," *Linc. Lab. J.* **15**(2), 165–180 (2005).

Biographies for the authors are not available.